Journal of Hydrology 603 (2021) 126920

Contents lists available at ScienceDirect

Journal of Hydrology

journal homepage: www.elsevier.com/locate/jhydrol

Research papers

Coastal flooding generated by ocean wave- and surge-driven groundwater fluctuations on a sandy barrier island

Rachel Housego [a,b,*], Britt Raubenheimer [b,*], Steve Elgar [b], Sandy Cross [c], Christian Legner [c], David Ryan [d]

[a] MIT-WHOI Joint Program in Oceanography, 266 Woods Hole Rd., Woods Hole, MA 02543, MS #12, USA
[b] Department of Applied Ocean Science and Engineering, Woods Hole Oceanographic Institution, 266 Woods Hole Rd., Woods Hole, MA 02543, USA
[c] Town of Duck, 1200 Duck Rd, Duck, NC 27949, USA
[d] Town of Nags Head, 5401 S. Croatan Hwy, Nags Head, NC 27959, USA

ARTICLE INFO

This manuscript was handled by Nandita Basu, Editor-in-Chief, with the assistance of Julianne Quinn, Associate Editor

Keywords:
Coastal hydrogeology
Flooding
Land-sea connection
Storms
Compound events
Citizen science

ABSTRACT

Three years of observations of groundwater elevations, ocean tides, surge, and waves, and rainfall are used to study coastal groundwater-driven flooding along the ocean side of a barrier island. Increases in surge and wave-driven water levels (setup) during 26 ocean storms with little rainfall, including the passage of 3 hurricanes, caused O(1 m) increases in groundwater heads under the dunes on the ocean side of the island, nearly double previously reported magnitudes. The inland propagation of the resulting pulses in groundwater levels is consistent with an analytical model (without recharge) based on shallow aquifer theory (Nash Sutcliffe model efficiencies of >0.7, maximum water-table level estimates within 0.1 m of observations). Infiltration of precipitation results in approximately a threefold increase in the groundwater level relative to the amount of rainfall. The analytical model (with recharge) driven with estimated ocean shoreline water levels (based on the 36-hr-averaged offshore tide, surge, and wave height) and measured precipitation predicts the maximum water-table height within 0.15 m of that observed across the barrier island during Hurricane Matthew, which was the only wave event during the 3-yr data set with more than 0.1 m rainfall.

Citizen-science reports from a smartphone app (iFlood) are used to evaluate the regional application of the model. Twenty-five ocean-side reports associated with 7 ocean storms (6 of which had minimal rainfall) between Sept 2019 and Feb 2020 showed flooding on natural (permeable) land surfaces along 70 km of the northern Outer Banks barrier island, from Corolla to Rodanthe, NC. The analytical model (with recharge) predicts flooding that is consistent with the timing and location for 19 of the 25 reports. Applying the model regionally suggests that more than 10% of the land area on the ocean side of the northern Outer Banks would be inundated by coastal groundwater even in the absence of rainfall for an ocean storm that generates a 2.25 m increase in the shoreline water level.

1. Introduction

Nearly 1.5 million people inhabit barrier islands along the U.S. Atlantic and Gulf Coasts with a population density approximately three times greater than that of coastal states (Zhang and Leatherman, 2011), which is increasing, along with the associated infrastructure (Elko et al., 2015). The low elevations (close to mean sea level, MSL) and high density of infrastructure make coastal counties susceptible to devastating environmental and economic impacts from flooding. In unconfined coastal aquifers, the average water table usually is higher than MSL and lies within a few meters of the land surface in low relief regions (Glover, 1959; Rotzoll and Fletcher, 2013; Befus et al., 2020). Although groundwater can cause flooding if the water table exceeds the land surface, groundwater processes typically are neglected in flood hazard mapping and management policies (Morris et al., 2007; Rotzoll and Fletcher, 2013; Abboud et al., 2018). As of 2019, the U.S. National Flood Insurance Program was ~$20 billion dollars in debt (Horn and Webel, 2019). Sea-level rise and the increasing strength and duration of

* Corresponding authors at: 266 Woods Hole Rd., Woods Hole, MA 02543, MS#12, USA (R. Housego). AOPE, 266 Woods Hole Rd., Woods Hole, MA 02543, MS#11, USA (B. Raubenheimer).
E-mail addresses: rhousego@whoi.edu (R. Housego), britt@whoi.edu (B. Raubenheimer), elgar@whoi.edu (S. Elgar), david.ryan@nagsheadnc.gov (D. Ryan).

https://doi.org/10.1016/j.jhydrol.2021.126920
Received 20 January 2021; Received in revised form 29 August 2021; Accepted 5 September 2021
Available online 11 September 2021

large wave and surge events (ocean storms) are predicted to double the frequency of flooding and to expand the spatial extent of flood impacts (Woodruff et al., 2013; Moftakhari et al., 2015; Vitousek et al., 2017; Patricola and Wehner, 2018; Befus et al., 2020; Knutson et al., 2020; Sweet et al., 2020). Compound flooding driven by multiple hazards, such as rain and storm surge, can magnify the duration and extent of flood impacts (Wahl et al., 2015; Bevacqua et al., 2019). Developing flood predictions that integrate oceanographic, meteorological, and hydrogeological processes has been identified as a research need for managing storm hazards and impacts (Elko et al., 2019). Increasing ocean storms that cause groundwater-driven flooding may require new management strategies, because traditional ocean-driven flood mitigation structures, such as jetties and sea walls, are ineffectual against increases in the water table. However, although several studies have analyzed impacts of sea-level rise on regional groundwater inundation and flooding (Rotzoll and Fletcher, 2013; Befus et al., 2020), regional effects of transient ocean storms are less well understood.

Prior studies of wave-and-surge-driven groundwater responses have focused on moderate wave conditions (Li et al., 2004; Trglavcnik et al., 2018; Rotzoll and El-Kadi, 2008). During ocean storm events, the elevation of the coastal water table fluctuates in response to changes in the wave-, tide-, and surge-driven changes in the ocean water level (Nielsen, 1990; Cartwright et al., 2004; Anderson and Lauer, 2008; Abarca et al., 2013). The resulting ocean-storm pulse increases the elevation of the coastal water table, and this bulge of high groundwater continues to propagate inland after the ocean water levels have subsided (Li et al., 2004; Rotzoll and El-Kadi, 2008). Ocean-storm pulses have larger amplitudes and longer fluctuation periods than water-table oscillations driven by wind waves or tides, and thus can penetrate farther into the aquifer (Nielsen, 1990; Li et al., 2004). As the ocean-storm signal propagates inland, the amplitude of the fluctuation attenuates at a rate controlled by the hydrogeologic properties and structural composition of the aquifer (Li et al., 2004; Rotzoll and El-Kadi, 2008).

An analytical solution (pulse model) assuming a vertical beach face and a homogeneous, isotropic, uniform-depth aquifer reproduced the behavior of a surge-and-wave-induced groundwater fluctuation in a sandy aquifer in a coastal barrier island (Cartwright et al., 2004; Li et al., 2004). However, the analytical model was developed and calibrated for a single event, and thus the model skill for multiple events and its applicability to other sites is uncertain. For example, leakage to the surface aquifer from a confined aquifer can result in non-uniform propagation of the storm pulse with smaller-than-predicted amplitude relative to the shoreline fluctuation (Trglavcnik et al., 2018).

When rainfall is coincident with emergent groundwater from the land surface, the duration of the flood tends to last longer than runoff- or overwash-driven flooding alone (MacDonald et al., 2008; Befus et al., 2020). The water table rises in response to infiltration from precipitation by an amount inversely dependent on the effective porosity of the aquifer (Meinzer, 1923; Crosbie et al., 2005; Cobby et al., 2009; Zhang et al., 2017; Smail et al., 2019). Antecedent conditions that result in an elevated water table reduce the aquifer infiltration capacity for subsequent events (Rotzoll and Fletcher, 2013).

Here, three years of continuous observations (Section 2), including 26 ocean storms with minimal rainfall, are used to evaluate the analytical storm-pulse model (Section 3) for the groundwater level in an unconfined surface aquifer driven by changes in the shoreline water level. The observed groundwater increases under the dune following large offshore wave events without precipitation (significant wave height, $H_s > 5$ m) are $O(1\text{ m})$, nearly double the amplitude measured in prior studies (Li et al., 2004; Rotzoll and El-Kadi, 2008; Trglavcnik et al., 2018), and similar in magnitude to the sea-level-rise (SLR)-driven groundwater increase predicted over the next hundred years (0.4–1.3 m of SLR predicted by 2100 off the coast of NC (Sweet et al., 2017)). The analytical model is shown to predict the maximum ocean-storm-driven groundwater levels within about 0.1 m and the timing of maximum groundwater levels within about 1 day. Using an estimated effective porosity, an analytical groundwater flooding model including the storm pulse and recharge is evaluated with measurements during the passage of Hurricane Matthew, which had wave heights >5.5 m, surge ~1.0 m, and precipitation ~0.2 m. Flood reports submitted to iFlood (Section 4.1), a citizen-science phone application, are used to conduct a hindcast assessment of the analytical groundwater-flooding model along a 70-km region of the Outer Banks between Corolla and Rodanthe, NC (Section 4.2). The analytical flooding model is used to predict regions of groundwater flood vulnerability on the ocean-side of the Outer Banks caused by an increase in the shoreline water level consistent with a hurricane or large Nor'easter (Section 4.3). Offshore wave heights and precipitation amounts that drive the analytical model are among the most ubiquitous measurements collected in global coastal observational arrays. Consequently, the framework presented here could be used to study regional groundwater-driven flooding in other low-lying coastal environments where the aquifer properties are roughly uniform.

2. Field measurements

Although this study is conducted on the North Carolina Outer Banks, the results are applicable to many other coastal areas. Sandy coasts account for about 33%, and sandy barrier islands account for ~7%, of global coastlines (Stutz and Pilkey, 2011; Vousdoukas et al., 2020). Furthermore, large sections of the U.S. Atlantic and Gulf coasts have coastal plain geology similar to the NC Outer Banks (USGS, 2017), for which the regional aquifer structure often can be approximated as homogeneous despite smaller-scale heterogeneity, similar to prior studies examining groundwater inundation driven by sea-level rise (Rotzoll and Fletcher, 2013; Befus et al., 2020).

2.1. Site description

The North Carolina Outer Banks is a 320-km long chain of barrier islands extending south from the Virginia-North Carolina state line to Bogue Inlet. The islands are up to 3-km wide, and have ocean-shoreline dunes from less than 1- to 12-m high (Elko et al., 2002). The North Carolina Outer Banks is part of the North Carolina Coastal Plain aquifer system, and the shallow geology is a 50–70 m thick Quaternary sequence that fills the Albemarle Embayment (Winner and Coble, 1996; Lautier, 2009). The surficial aquifer typically is comprised of >70% sand (Winner and Coble, 1996). A network of paleo-channels that were backfilled with younger Pleistocene sediments also weaves through the Quartenary sequence (Riggs et al., 1995; Lazarus and Murray, 2011). The paleo-channels contain muddy estuarine sediment, sand, and fluvial gravel (Lazarus and Murray, 2011). Branches of the paleo-Roanoke/Albemarle fluvial system have been recorded at the shoreface in Duck, Kitty Hawk, Kill Devil Hills, and Nags Head (Riggs et al., 1995; Boss et al., 2002; Lazarus and Murray, 2011). The surficial aquifer is underlain by a series of discontinuous clay and silt beds that comprise the Yorktown confining unit, which is estimated to occur 15–20 m below NAVD88 (approximately mean sea level) (Winner and Coble, 1996; Mallinson et al., 2010). Similar to many barrier island areas, land use is primarily single family residential with houses on stilts (~65% total land with lot coverage <33%) or shared-open-use (common, vacant, or public, ~24% total land area with primarily pervious surfaces). In addition, topographic relief is low, especially in developed areas, and surface runoff is expected to be minimal.

In September 2014, 19 groundwater wells were installed at 8 locations along a 550-m-long transect across the barrier island extending from the ocean dune to the sound at the U.S. Army Corps of Engineers Coastal Hydraulics Laboratory Field Research Facility (FRF, http://www.frf.usace.army.mil) in Duck, NC (Fig. 1). The property is bordered on the west by Currituck Sound and on the east by the Atlantic Ocean. On the ocean-side of the island, the beach is backed by ~7-m-high vegetated dunes. Sediment samples collected during construction of the FRF facility (Meisburger et al., 1989) and during installation of the

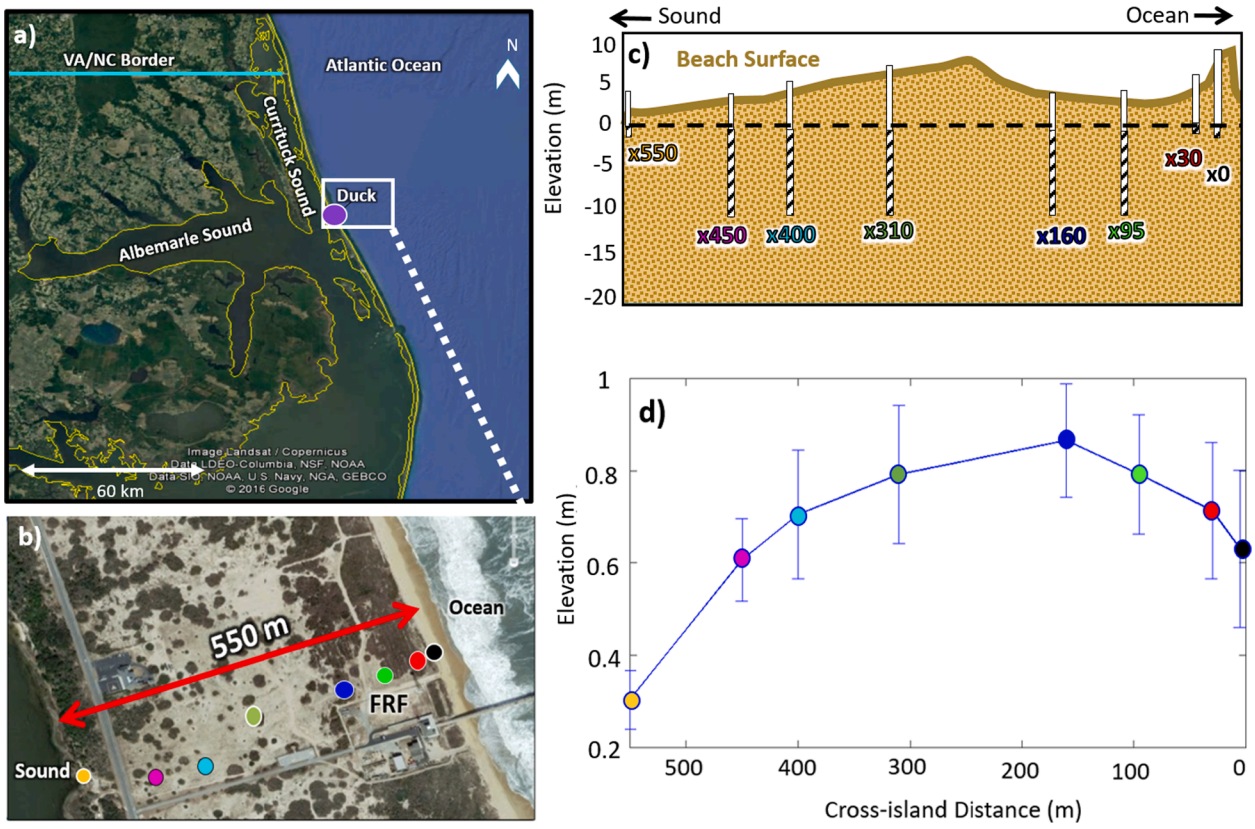

Fig. 1. a) Google Earth image of northeastern North Carolina, including the Outer Banks. The land is outlined in yellow. The U.S. Army Corps of Engineers Field Research Facility (FRF, purple circle in the white box), Duck, NC is located on a barrier island between Currituck Sound and the Atlantic Ocean. b) Close-up view of the barrier island showing the locations of groundwater wells (colored circles) extending from the ocean dune to the sound. c) Elevation of the beach surface (tan curve) relative to NAVD88 and groundwater wells (long, thin white rectangles) versus distance from the well closest to the ocean. The cross-hatched region on each well is the screened section. The horizontal dashed black line is 0 m NAVD88. d) Annual average water-table elevation versus cross-island distance. The vertical bars represent 1 standard deviation. (For interpretation of the references to color in this figure legend, the reader is referred to the web version of this article.)

groundwater wells suggest that the surficial aquifer is composed of medium quartz sand (mean diameter ~0.25 mm) and shell hash. Prior studies suggest the uppermost confining layer is roughly 15 to 30 m below NAVD88 (Meisburger et al., 1989; Manahan et al., 1998). However, a confining unit was not encountered during drilling, with boreholes extending from 15 (under the dune) to 26 m (near the sound) below NAVD88. Slug tests (Hvorslev, 1951; Bouwer and Rice, 1976; Brown et al., 1995; Butler et al., 1996) performed at 16 of the wells spanning the island suggest that the hydraulic conductivity is approximately $K = 13.0 \pm 4.4$ m/d, consistent with an estimate of 14.9 m/d obtained during drilling of a test water supply well about 2 miles south of the study site (Manahan et al., 1998). Based on these observations, the aquifer is assumed to be approximately uniform across the island.

2.2. Observations

The cross-shore positions (x, positive toward the sound) of the well locations are defined relative to the well closest to the dune face. Each well was composed of 0.05 m-diameter PVC pipe with No.10 perforated screen at the bottom surrounded by gravel pack topped with a bentonite seal. At the six mid-island locations (Fig. 1c, $95 \leq x \leq 450$ m), wells extended to 9 to 10 m below NAVD88 with 8- to 9-m-long screens. Near the ocean (Fig. 1b, red and black circles) and sound (Fig. 1b, orange circle), wells (Fig. 1c) extended to about 1 m below NAVD88 with 0.6-m-long screens (Fig. 1c). Conductivity-temperature-depth (CTD) sensors at about mid-screen-elevation in each well were sampled at 10-min intervals. Salinities were less than 1 PSU, except in the well closest to the ocean (x0) following large ocean storms when saline ocean water penetrated under the dune (Fig. 1c, x0). Water density was calculated from the measured salinity, temperature, and pressure (Fofonoff and Millard, 1983). Measurements collected by slowly lowering a CTD within each well showed that density was approximately vertically uniform. The sensors were vented to the atmosphere so that pressure measurements were not influenced by fluctuations in barometric pressure. Sensor elevations were estimated using differential GPS measurements of the well cap, and simultaneous water-level measurements (from a standard meter) and pressure and water density measurements from the in situ sensors. Annual re-estimates show <0.02 m drift. Water table elevations were estimated from the pressure measurements converted to head h as (Post et al., 2007, Equation (5)),

$$h = \frac{p}{\rho_f g} + z_s \tag{1}$$

where p (Pa) is the measured pressure, ρ_f (kg/m^3) is the density of freshwater, g (m/s^2) is the gravitational constant, and z_s (m) is the elevation of the sensor (relative to NAVD88). Assuming a reference level z_r of 0 NAVD88, the largest deviations from (1) owing to density differences (Post et al., 2007, Equation (12)) at x0 are less than 0.01 m.

Ocean water levels were measured every 6 min with a NOAA tide gauge (ID **8651371**) in about 6 m depth at the end of the FRF pier. Tides were semi-diurnal with range ~1 m and storm surge was up to ~1 m. Significant wave heights (H_s, 4 times the standard deviation of sea-surface elevation fluctuations in the frequency range from 0.05 to 0.30 Hz) recorded every 30 min in 26-m water depth (NDBC Station **44100**) ranged from near 0 to 6 m (Fig. 2a), with an average of about 1 m. Breaking wave-driven setup (Longuet-Higgins and Stewart, 1964) of the shoreline water levels is estimated to be 0.2 times the offshore

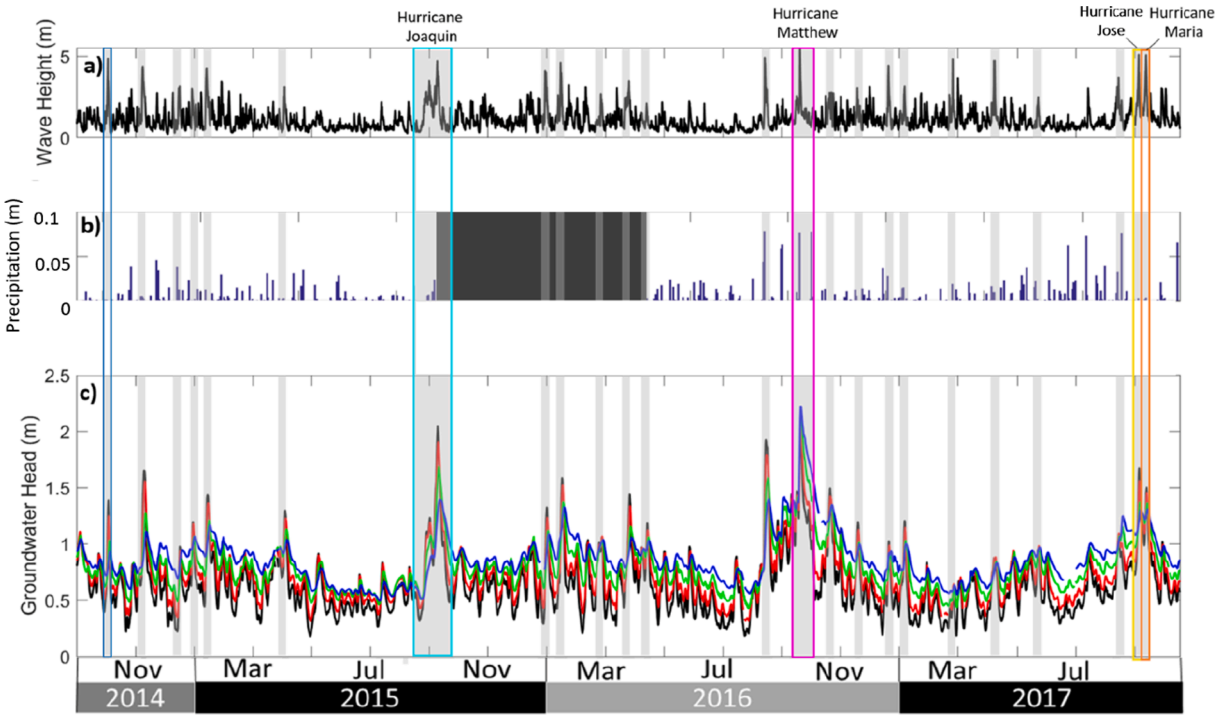

Fig. 2. a) Significant wave height, b) precipitation, and c) 36-hr average freshwater equivalent groundwater head (x = 0, 30, 95, 160 m, black, red, green, blue curves) versus time. Colored boxes identify periods with impacts from a nor'easter (dark blue, Oct. 2014) and Hurricanes Joaquin (light blue, Oct. 2015), Matthew (magenta, Oct. 2016), Jose (yellow, Sept. 2017) and Maria (orange, Sept. 2017). Vertical grey shaded areas indicate the 27 wave and surge events (ocean storms) during the 3-yr period. The precipitation gauge was not operational between Sept. 2015 and May 2016 (black box 2b). (For interpretation of the references to color in this figure legend, the reader is referred to the web version of this article.)

significant wave height (Guza and Thornton, 1981; Nielsen, 1988; Raubenheimer et al., 2001), roughly consistent with observations from a lidar on the dune about 300 m north of the wells. Shoreline water levels are estimated as the sum of the ocean water level (including tides and surge) and the setup.

Ocean storms are defined as events with combined 36-hr averaged (de-tided) shoreline water level exceeding 0.65 m above NAVD88. Twenty-seven ocean-storm events were observed during the 3-year data record, including 4 hurricanes that passed offshore of Duck, NC (Joaquin, Oct. 2015 (cyan box, Fig. 2), Matthew, Oct. 2016 (magenta box, Fig. 2), and Jose and Maria, Sept. 2017 (yellow and orange boxes, Fig. 2, respectively)).

Precipitation (Fig. 2b) was recorded every 10 min using a set of 3 rain gauges. Data from the precipitation gauges is uncertain during extreme rainfall rates (>0.03 m/hr), which only occurred once in the observation period (during Hurricane Matthew, Oct. 2016). With the exception of Hurricane Matthew, there was <0.1 m rainfall during the ocean storms. Tidal effects were negligible in the sound, but winds can drive rapid 1–2 m changes in the sound water level (Mulligan et al., 2014). Low sound water levels typically occur during the winter months (Caldwell, 2001) and often are coincident with high ocean water levels driven by winter storms. Under calm conditions the ocean-side groundwater heads increase landward (Fig. 1d and Fig. 2c, blue and green curves are higher than red and black curves, e.g., May-July 2015), and the water table is highest ~160 m inland from the dune (Fig. 1c, d). The average head gradient between the center of the island and the ocean well (x0) is 0.0015 m/m (Fig. 1d). However, during storms, surge, setup, and wave infiltration result in the groundwater head at the wells closest to the ocean exceeding the head levels at the inland wells (Fig. 2c, shaded grey areas, and Fig. 3). The bulge of high groundwater attenuates as it propagates inland (Fig. 3b, solid curves).

The two storms that resulted in the highest groundwater levels at x0 were Hurricane Joaquin (cyan box, Fig. 2) and Hurricane Matthew

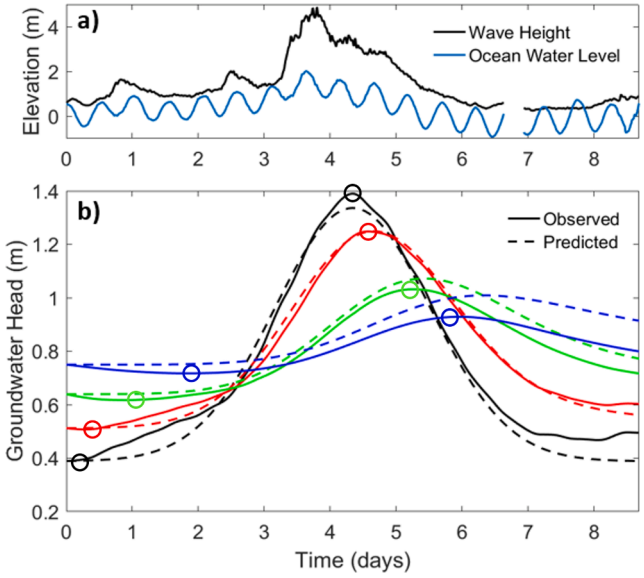

Fig. 3. a) Significant wave height (black) and ocean water level (blue) and b) 36-hr average freshwater head observed (solid curves) and predicted using pulse theory (Li et al. 2004, dashed curves) with D = 3500 m^2/d versus time for a single nor'easter (dark blue box Fig. 2) at x = 0, 30, 95, 160 m (black, red, green, blue curves). Open circles mark the start and end of the observational data used to fit the Li et al. (2004) model. (For interpretation of the references to color in this figure legend, the reader is referred to the web version of this article.)

(magenta box, Fig. 2). A nor'easter preceded Hurricane Joaquin and caused sustained elevated offshore wave heights. Soon after the nor'easter, Hurricane Joaquin developed in the Atlantic and generated a

second series of large waves that reached maximum heights of 4.7 m in 26-m water depth on October 5, 2015. Head levels increased 1.6, 1.4, 1.2, 0.9 m above pre-storm levels during Hurricane Joaquin at x = 0, 25, 90, and 160 m, respectively (Fig. 2c) and 0.5 m at x = 310 m (not shown). When the high water levels from Hurricane Joaquin propagated inland, the water table came within approximately 1 m of the ground surface at x95 and x160. Following Hurricane Joaquin, the water table at x160 took approximately two weeks to return to within a standard deviation of the average level. The time delays between the occurrences of maximum water levels at each well location indicate an inland propagation rate of the storm-driven groundwater bulge of about 60 m/day.

During Hurricane Matthew, infiltration from heavy precipitation (>0.2 m, FEMA 2018 Table 3) and increasing ocean water levels both contributed to the increase in the water table. Instead of a delayed response in the time of arrival of the maximum water level, a near simultaneous 0.6 to 0.9 m increase in groundwater level occurred at all well locations (Fig. 2) following the heavy precipitation.

3. Analytical model

3.1. Groundwater-pulse theory evaluation

Propagation of the storm-driven groundwater pulse is simulated using an analytical solution (referred to subsequently as the analytical model (no recharge)) (Li et al., 2004) for Darcian groundwater flow assuming a Gaussian shoreline fluctuation (pulse) and applying a linearization based on the assumption that the amplitude of the water-table fluctuation is small relative to the depth of the aquifer (see Appendix). Here, the propagation is driven (Equation (A1)) with the head fluctuations at the x0 well rather than with the shoreline fluctuations to avoid errors resulting from uncertainty in the cross-shore position of the shoreline, which changes with changing ocean water levels on the sloping beach, with evolving beach topography during storms (up to 4 m erosion during a single event), with seasons (the mean shoreline position can vary 10 s of meters as the beach accretes during the summer and erodes during the winter), and with long-term trends (the dune eroded more than 10 m landward during the observation period). The model is solved numerically using global adaptive quadrature with an absolute error tolerance of 1e-12 m and a time step of 0.01 days. Tests with smaller time steps were conducted to ensure the solution was robust. Errors from the numerical integration scheme do not contribute significantly to the model uncertainty ($\ll$ 0.001 m). The fits between the water table levels for the 26 observed storm pulses with minimal rainfall and a Gaussian shape had correlations $R^2 > 0.9$, although 5 storms were negatively skewed, and 10 storms were positively skewed, with 5 skewness magnitudes >0.3.

Data from the four wells closest to the ocean (x0-x160) during the 26 storms with minimal rainfall are included in the evaluation of the pulse theory. The best-fit diffusivity for storm pulses is $D = 3500$ m^2/d, which is within a factor 2 of the diffusivity based on the estimated hydrologic parameters (hydraulic conductivity $10 < K < 30$ m/d, specific yield $S_y = 0.3$, and the aquifer depth $15 < z < 30$ m). The analytical model (without recharge) reproduces the observed surge- and wave-driven changes in the water table well to very well based on the Nash Sutcliffe Efficiency (NSE, Nash and Sutcliffe, 1970) coefficients (Table 1). The model agreement with the observations often is worse at x0 than at x30 or x95 owing to greater deviations from a Gaussian fit (compare solid with dashed curves in Fig. 3, which shows an example for a single storm). Differences between the observed and theoretical groundwater levels are larger after the storm peak (Table 1, NSE are larger for the entire event than for just the rising portion, and Fig. 3), at least partly because deviations from a Gaussian are larger during the waning ocean storm. The root mean square error (RMSE) between the analytical and observed maximum water table (which is used to estimate regional flood occurrences) is ~0.1 m at all locations for all storms, and the estimated timing of the maximum water level is correct to within 0.5 days.

Table 1
Average Nash Sutcliffe Efficiency coefficients (±std. dev.) for the analytical model without recharge for the 26 ocean storms with minimal rainfall at the cross-shore locations of the four wells closest to the ocean. Event values include both the rising (e.g., identified by circles in Fig. 3) and falling (until 7 days after the peak water table levels) portion of the storm pulse.

	Nash Sutcliffe Efficiency (NSE) coefficient (±std. dev.)	
Location	Ocean storm event	Rising water table only
x0	0.73 ± 0.16	0.87 ± 0.12
x30	0.77 ± 0.14	0.91 ± 0.10
x95	0.79 ± 0.16	0.91 ± 0.11
x160	0.71 ± 0.20	0.83 ± 0.15

The inland amplitude decay and phase evolution of the ocean-storm-pulse fluctuations are used to examine the model-data agreement further. The non-dimensional model (Equation (A3)) is solved numerically for $0 < x^* < 1.5$ with 0.01 resolution. Analytical estimates (Fig. 4, solid curves) of the bulge properties (α and $\Delta\phi_*$) as a function of inland distance x^* are obtained from the magnitude and time of the maximum of the non-dimensional Gaussian pulse at each cross-shore position (Equation (A3)). Observational estimates of the non-dimensional amplitude attenuation, phase lag, and distance (Fig. 4, symbols) are estimated from Equations (A4-A7), with A, A_j, t_p, t, and B_j determined from the best fits of the measured groundwater levels h to Gaussian curves (Equation (A2)). The agreement between the model and observed non-dimensional amplitude attenuation α and phase lag $\Delta\phi^*$ (correlations $R^2 = 0.73$ and 0.71, respectively) is insensitive to cross-shore distance (Fig. 4), consistent with the assumption that the aquifer at Duck is approximately homogeneous and isotropic (Li et al., 2004).

3.2. Precipitation response

The change in the water table from precipitation-driven recharge scales with the effective porosity, n_e. For sand, porosity, n, is estimated

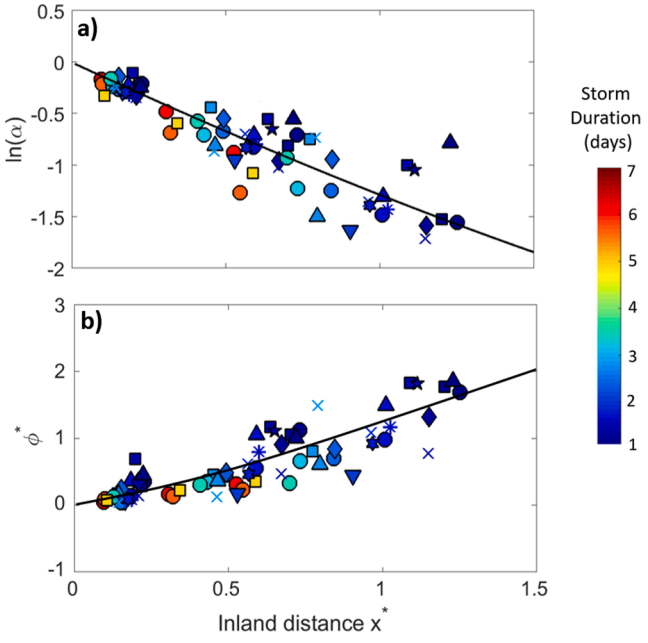

Fig. 4. Observed (symbols) and theoretical (black curves, Li et al., 2004, Equation A2) a) non-dimensional amplitude attenuation and b) phase change versus normalized inland distance. Symbol shapes correspond to different storms (n = 26), with colors corresponding to storm duration (color scale on the right). The squared correlation R^2 between observations and theory is 0.73 and 0.71 for amplitude attenuation and phase change, respectively.

to range from 0.36 to 0.43, and $n = 0.4$ for grab samples collected in the intertidal zone at Duck. To estimate the value of the effective porosity, the groundwater data on the sound side of the island (x310 to x550, Fig. 1), where ocean-driven groundwater fluctuations typically are negligible under low wave conditions, are used to determine the water-table response to precipitation events. Rainfall events (separated by dry periods longer than 2 days) between Oct 2014 and Oct 2016 with cumulative precipitation >0.02 m are included in the analysis. The water table increase is approximately three times the amount of rainfall at all sites (Fig. 5 for x = 310, 400, and 450 m), corresponding to an effective porosity n_e of about 0.33, roughly consistent with porosity estimates for sand. The analytical model with recharge reproduces the maximum water table levels during Hurricane Matthew (assuming 0.2 m rainfall) within about 0.15 m and the time of maximum water table level within 0.2 days.

4. Flooding on the North Carolina Outer Banks

4.1. iFlood citizen science app

A citizen-science phone application (app), iFlood, was released in September 2019 to collect flood information, including location, depth, recent rainfall, and photographs on the North Carolina Outer Banks (Fig. 6). Here, the flood reports are used to validate the combined pulse-and-recharge flooding model (Equation A8) for the Outer Banks region. When a flood report is submitted, the GPS position of the phone and the position of a drop pin that can be moved manually on the map screen are recorded (Fig. 6). The user can send a photograph of the flood, answer survey questions about the flood depth, location, and recent rainfall, and provide additional comments, with the data stored on a cloud-based Firebase server. The app was advertised on town social media pages, in local newsletters, and on an NSF repository for citizen science projects, and was presented at an OBX Green Drinks chapter meeting. When possible the approximate position of the reported location was validated by comparing images in Google Earth street view with the photograph submitted to the app. Reports with unrealistic locations (e.g. several reports submitted to iFlood had locations in the middle of the Atlantic) were eliminated during the quality control process. About half the reports were submitted by town managers and research partners at the USACE FRF.

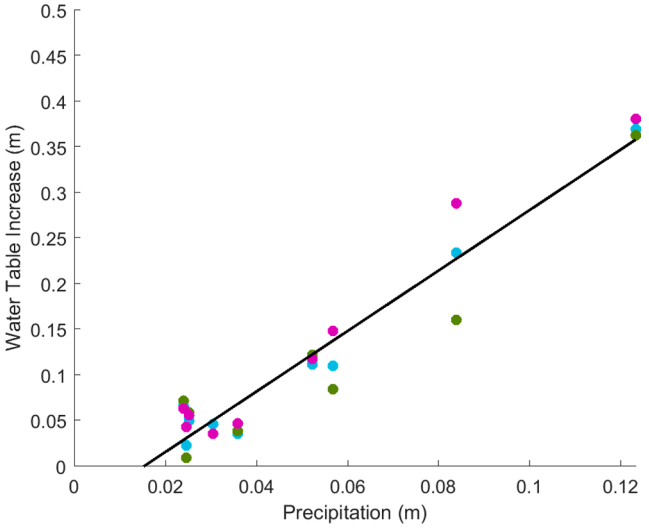

Fig. 5. Increase in water-table elevation versus total rainfall at x = 310 (light blue), 400 (green), and 450 m (pink) (colors match the colors of the wells in Fig. 1) for rainfall events with cumulative precipitation >0.02 m. The solid line is a linear least squares fit (squared correlation $R^2 = 0.74$) forced through zero, with slope ~3. Data points with Studentized residuals >3 were removed as outliers. (For interpretation of the references to color in this figure legend, the reader is referred to the web version of this article.)

Between September 2019 and February 2020, 34 quality-controlled reports associated with at least 7 storms (including Hurricane Dorian in Sept 2019) indicated flooding between Corolla and Rodanthe, NC (Fig. 7). Oceanside flooding occurred up to 5 days after storms with ocean surge up to 1.0 m, significant wave heights in 26-m depth from 3.5 to 7.0 m, and cumulative daily rainfall ranging from negligible to 0.15 m (Fig. 8, purple box, dates before December 2019). The most reports (16) associated with a single event occurred following Hurricane Dorian (Fig. 8). Sound water level changes may have contributed to flooding on the sound side of the barrier island (Fig. 8, orange box, after December 2019). There were no sound water level measurements during this period, and thus the 6 sound-side flood reports were not analyzed. Three additional flood reports were excluded because the report photo suggested that the flooding resulted primarily from ponding on impermeable surfaces (e.g., roadways).

4.2. Regional flood hindcasts

The location and timing of the remaining 25 ocean-side flood reports are compared with the analytical estimates of the groundwater-rain-induced flooding (2 examples are shown in Fig. 9). The analytical model with recharge is driven with precipitation measured at the FRF (assuming all land surfaces are pervious) and the approximate ocean shoreline water level estimated as the 36-hr-running-average of the sum of the offshore tide, surge, and shoreline setup. The cross-shore distance (x) is measured from the estimated dune position, and the land surface elevation is determined from a 5x5 m digital elevation model (DEM) measured by the Joint Airborne Lidar Bathymetry Technical Center of Expertise (JABLTCX) in Fall 2019. The pre-storm water table at the dune (x0) is estimated to be 0.3 m based on the in situ observations, roughly consistent with the overheight expected for a 1-m amplitude semi-diurnal tide on a 0.1 slope (Nielsen, 1990; Raubenheimer et al., 1999). Inland of the shoreline the pre-storm water table is estimated using the annual average gradient (0.0015 m/m) between the x0 and x160 wells. The diffusivity is assumed to be uniform throughout the surface aquifer (see Discussion).

Each storm event is simulated separately because the model has less skill at predicting post-storm recovery and is invalid after the water table exceeds the land surface. Based on the aquifer recovery times in the Duck field observations, the groundwater levels typically return to near those expected without a storm within 2 weeks, so estimating storms separately during some closely spaced events would have higher uncertainties than considered in the hindcast evaluation. The uncertainty of the analytical model with recharge is estimated as 0.3 m and includes uncertainty for the maximum water table elevation driven by a rise in shoreline water level (RMSE error 0.1 m), uncertainty of the pre-storm water table position (±0.05 m, standard deviation of the mean water table position observed at the dune well (x0), which had the highest variance in water level), and uncertainty in the land surface position based on the vertical resolution of the lidar measurement (±0.15 m).

The analytical model with recharge predicts a flood (i.e., the predicted water table exceeds the land surface within the model uncertainty of ±0.3 m) that is consistent with the report timing (±1 day) and location for 19 of the 25 flood reports, for storms with and without precipitation (Fig. 10, data points are in or above the pink shaded region). The one-day window was selected for validation because flooding may have occurred prior to the time the report was submitted, and cumulative precipitation is applied to the analytical model with recharge at the end of each day. All reports that are not predicted as flooding events by the analytical model with recharge were made following Hurricane Dorian, which was the only event with heavy precipitation (total rainfall ~0.17 m) during the regional study (dark blue squares Fig. 10), making it difficult to evaluate the model's performance for combined surge-and-rain processes. Three of the Dorian reports (with

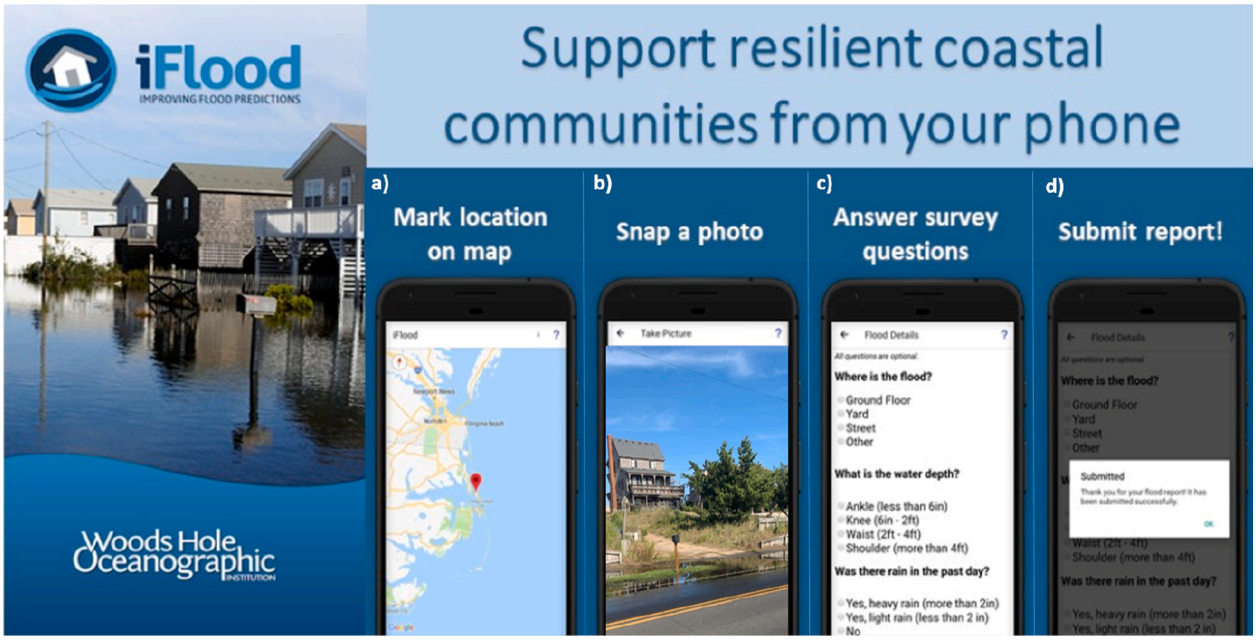

Fig. 6. Screenshots showing the user interface in the iFlood app. a) map screen b) photo screen c) survey questions screen d) submission screen.

predicted water table position ~−0.5 m) were located >200 m inland where uncertainty may be larger, and a 4th report had an unusually high land surface elevation (predicted water table position −1.3 m). Surface ponding associated with precipitation that is decoupled from the groundwater behavior (i.e., infiltration limited) may explain the discrepancy between the observed and predicted flooding during Hurricane Dorian.

For most of the events, the surge-driven pulse dominates the groundwater response. Specifically, the pulse hindcasts suggest up to 0.5 m ocean-driven groundwater increases for no rain (gray symbols Fig. 10, compare the initial with final groundwater position), and roughly 0.6 m ocean-driven increases during light (typically < 0.02 m, Fig. 8) rain events (light blue symbols Fig. 10, hindcast water table increases of up to 0.7 m with less than 0.1 m increase owing to recharge). Additionally, inaccuracy in the report locations, uncertainty in the initial water table configuration, and errors in the land surface elevation also could contribute to model-data discrepancies (see Discussion).

4.3. Regional flood vulnerability forecasts

The analytical model is applied to two hypothetical storms with ~7 day periods (time coefficient B = 0.3, Equations (A1) and (A2)), including a moderate storm with a 0.90 m increase in the shoreline water level (amplitude A = 0.90) which was the average for the observed storms, and an extreme storm during which the shoreline water level increased 2.25 m, to assess the vulnerability of the Outer Banks to flooding during future storms. Ocean storms of greater or equal magnitude to the moderate case have occurred 313 times between 2009 and 2019, while wave heights consistent with the extreme storm case have only occurred once during that interval. In both cases, it is assumed that there is no wave overtopping of the dune. The analytical model is applied to every grid cell in the JABLTCX DEM, extending to the lesser of the midpoint of the barrier island or 600 m inland for each cross-island transect. Beyond 600 m, the fluctuation in the water table associated with the change in the offshore water level is negligible (<0.1 m). The amount of rainfall needed to flood each grid cell is determined from the effective porosity and the difference between the maximum water-table elevation and the land surface assuming the land surface is pervious. Variation in land surface type was not considered, but will influence only recharge, not the wave-and-surge driven increases in the water table (see Section 5.2). Flooding is assumed to be constrained to the area within the grid cell, and does not affect adjacent cells.

In the extreme storm case, over 10% of the land area is flooded as a result of the increased shoreline water level and resulting propagation of the groundwater pulse (Fig. 11a, b). A large band of flooding occurs along the NC-12 highway where the low elevation of the roadway coincides with large increases in the water table owing to the proximity of the shoreline (Fig. 11b). Inland flooding is patchier and coincides with regions of low ground elevation. For the moderate storm case, 1.6% of the land area is flooded owing to the groundwater pulse (Fig. 11c).

The locations of flood reports coincide with areas predicted to have high flood vulnerability for these storm cases (Fig. 11). As a result of low land elevations, northern Duck and Rodanthe are predicted to have the highest vulnerability to coastal groundwater flooding. Most of the barrier would be flooded if precipitation amounts were ~0.8 m (Fig. 11, all except black areas). The groundwater pulse amplitude scales linearly with the shoreline fluctuation amplitude (Equation (A1)), and thus increasing wave height or storm surge increases flooding proportionally. In contrast, the groundwater pulse amplitude scales with the square root of the storm duration (Equation (A1)), and thus flooding is relatively insensitive to storm period. Doubling the storm duration results in <1% change in the flooded area.

5. Discussion

5.1. Model assumptions and limitations

Errors in the modeled maximum water table partly may be a consequence of neglecting overland flows during heavy rainfall. The model does not account for surface–subsurface exchange and is not valid after the water table exceeds the land surface. Additionally, the model reproduces the maximum water table height more accurately than it reproduces the timing of flooding. Timing errors may result from neglecting the asymmetries in the rise and fall of the shoreline water levels. If the shoreline rises faster than it falls, the pulse period (and thus pulse amplitude attenuation and phase lag with inland distance, Fig. 4) would be under-estimated, and flooding would occur earlier than predicted. Timing errors also may result from modeling the rainfall as an instantaneous increase in the water table level, rather than accounting for the time history of rainfall-induced infiltration (Broadbridge and

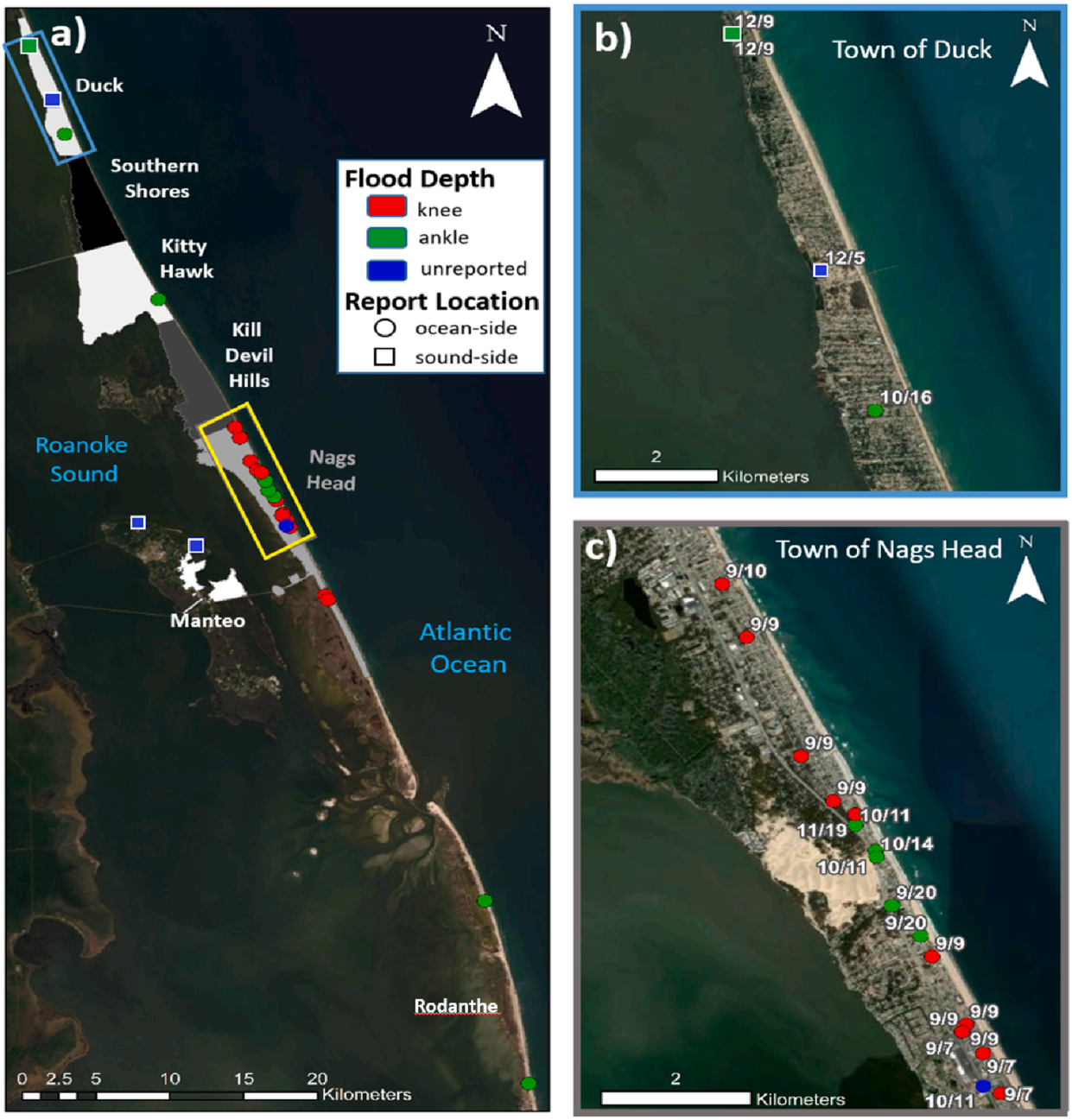

Fig. 7. a) Map of iFlood app report locations (symbols), and zoomed-in regional maps of reports in b) Duck (extent indicated by blue box in panel a) and c) Nags Head (yellow box in panel a). Marker colors indicate the reported flood depth (knee-high = red, ankle = green, unreported = blue), shape indicates ocean (circle) or sound (square) side of the island, and numbers indicate the date (MM/DD) the flood was reported. (For interpretation of the references to color in this figure legend, the reader is referred to the web version of this article.)

White, 1988) and of the groundwater drainage (recovery) following the precipitation. Variation in land surface type also could influence recharge patterns and was not considered. It might be possible to reduce timing errors by including recharge effects in areas with extensive historical monitoring.

Although the analytical model assumes that the diffusivity of the surface aquifer is spatially uniform, the presence of paleochannels suggests that there is some heterogeneity in the alongshore direction (Browder and McNinch, 2006; Mallinson et al., 2010; Lazarus and Murray, 2011), which can introduce errors in the predicted water level and cause deviations from the simple one-dimensional framework. The diffusivity affects both the steady-state pre-storm head gradient and the amplitude attenuation of the pulse. For example, an increase in the hydraulic conductivity or the aquifer depth would decrease the pre-storm head gradient, but also would increase the maximum fluctuation amplitude at a given location because the storm pulse will attenuate less quickly with inland distance (Fig. 4, $\ln(\alpha)$ increases with decreasing x^*, which is inversely proportional to $D = Kz/S_y$, Equation (A7)). Thus, a 50% change in aquifer diffusivity is expected to cause <5% change in the maximum water table elevation. However, alongshore variation in the diffusivity could result in alongshore flows and gradients that are not included in the cross-island system considered here.

Vertical variation in the location of the confining bed can influence the cross-shore structure of the water table (Anderson et al., 2000), but these variations are expected to be small relative to the groundwater level changes resulting from the storm pulses. Connections between the

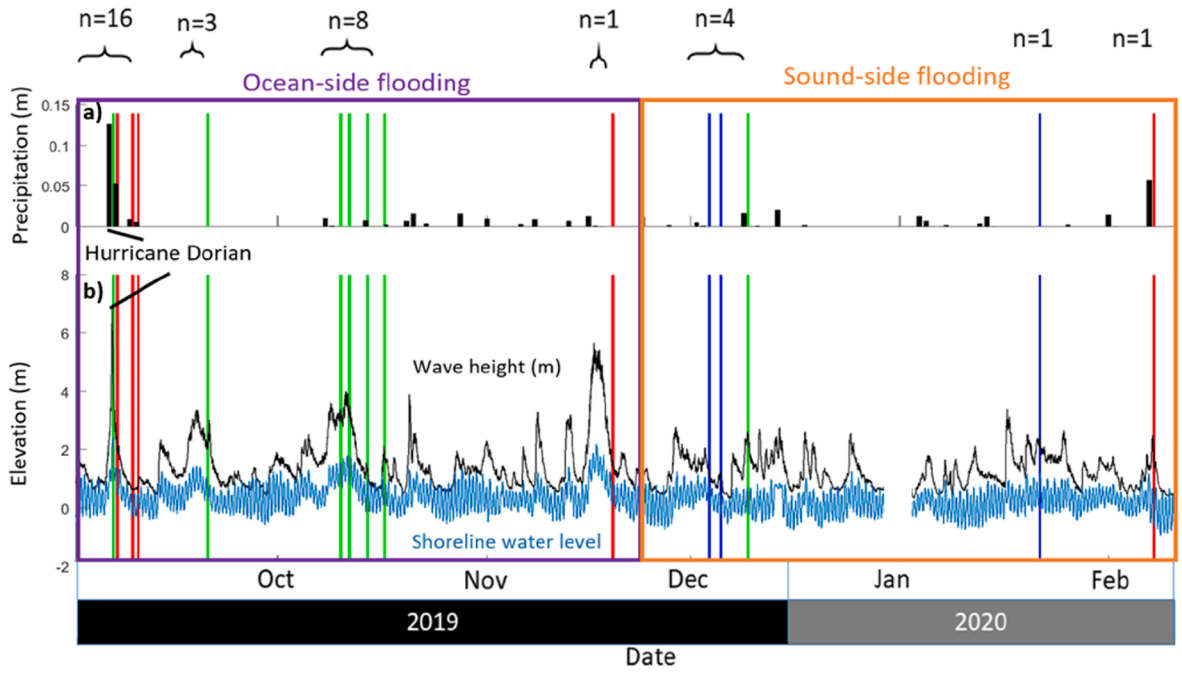

Fig. 8. a) Precipitation (black bars) and b) offshore significant wave height (black curve) and shoreline water level (blue curve) versus time, with timing of flood reports (indicated by the vertical lines with colors representing reported flood depth (knee-high = red, ankle = green, unreported = blue). The number above the event indicates the number of reports. The purple box (before December 2019) indicates flood reports from the ocean side of the barrier, and the orange box (after December 2019) indicates flood reports from the sound side of the barrier. (For interpretation of the references to color in this figure legend, the reader is referred to the web version of this article.)

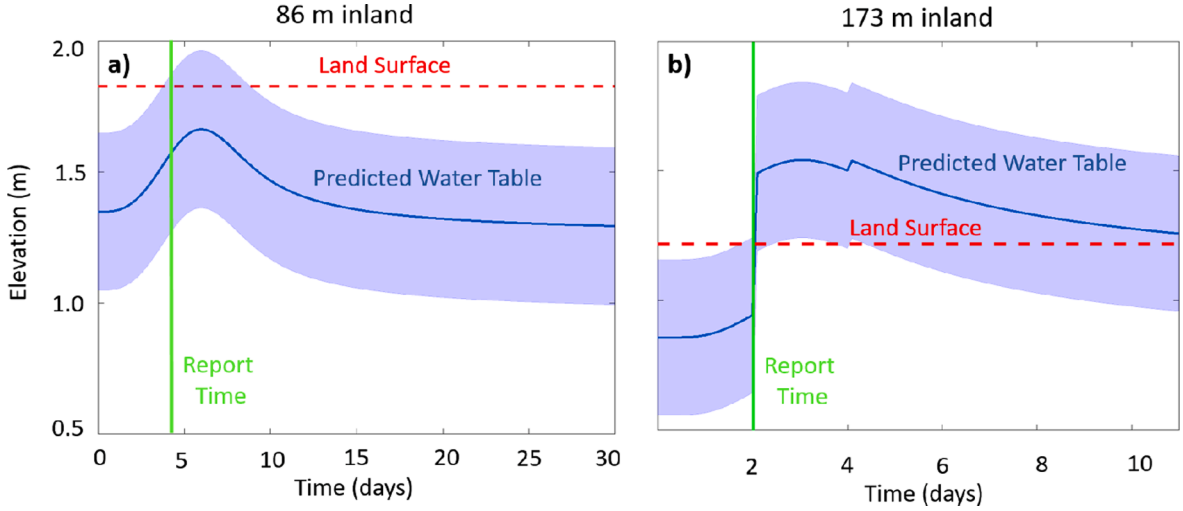

Fig. 9. Predicted water-table elevation (blue curve, with estimated model uncertainty (±0.3 m) shown by the blue-shaded region) versus time for an event with a) no rain (ocean surge and setup only) and an event with b) heavy rain at the start of day 2. The vertical green lines indicate the time a flood report was submitted, and the horizontal red-dashed lines indicate the elevation of the land surface. For both cases, the predicted water-table elevation (within the blue-shaded model uncertainty range) exceeds the land surface at the time the flood report was submitted. (For interpretation of the references to color in this figure legend, the reader is referred to the web version of this article.)

surface aquifer and subsurface confined aquifers also would result in deviations from the storm pulse solution (Trefry and Bekele, 2004; Trglavcnik et al., 2018). The skill of the analytical model with recharge at predicting flooding consistent with the iFlood reports suggests that aquifer heterogeneity has a relatively small effect on the pulse propagation on the ocean-side of the barrier island. It also was assumed that there was a constant head gradient prior to the storm, and that the groundwater divide is mid-island and does not vary with time.

Sound-side flooding was not considered in this analysis, owing to the lack of sound water level measurements. Increases in the sound water levels likely produce inland propagating groundwater bulges, similar to those on the ocean side, as well as overtopping shorelines and inundating low-lying sound-side neighborhoods. However, changes in the sound water level are better approximated as a step-function (rapid increase with a slow decline) than a Gaussian (Caldwell, 2001). In areas where the island width is narrower than the damping distance of the pulse, the sound-driven pulse will interact with the ocean-driven pulse to create more complex fluctuations in the water table, similar to interactions between tidal fluctuations that have been observed across narrow barriers (Huang et al., 2015; Colyar, 2016; Li et al., 2000). In

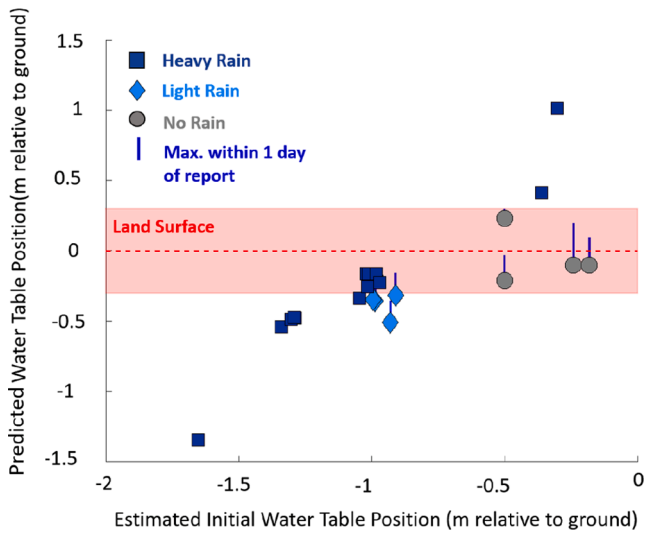

Fig. 10. Predicted water-table elevation at the report time versus estimated initial water-table elevation relative to the ground surface. Symbol shapes and colors indicate the reported precipitation (dark-blue square = heavy, light-blue diamond = light, gray circle = none). The vertical blue lines indicate the maximum elevation of the water table predicted within one day of the flood report. The dashed red line is the land surface and the shaded pink region is the model uncertainty. (For interpretation of the references to color in this figure legend, the reader is referred to the web version of this article.)

regions where sound water levels are available, it would be possible to develop an analytical model for flooding across the entire barrier island that incorporates sound and ocean water level fluctuations, as well as rainfall (Rotzoll et al., 2008).

5.2. *Relative importance of precipitation and shoreline-driven changes in the groundwater level*

During the three-year in-situ observation period there was only one instance when cumulative rainfall during a storm event exceeded 0.1 m (Hurricane Matthew precipitation ~0.2 m). Based on the estimated effective porosity, this precipitation would cause a corresponding increase in the groundwater head of about 0.6 m. Over the same period there were 18 times when increased shoreline water levels driven by waves and surge increased the water table under the dune >0.6 m, suggesting that along the North Carolina coast the wave-and-surge-driven processes are a more persistent challenge for managing coastal groundwater hazards than rainfall. However, recharge elevates the water table across the entire island (assuming a pervious land surface), while the wave-and-surge-driven water table increases are largest within several hundred meters of the ocean dune. Therefore, rainfall likely plays a larger role in driving groundwater flooding on the sound side of the island, where the wave-and-surge signal has attenuated and land surface elevations are lower (the water table is closer to the land surface and a smaller increase in the water table is needed to cause flooding).

Recharge and wave-and-surge-driven increases in the water table were treated as additive in the analytical model with recharge (Equation (A8)). This approach reproduced the maximum water level observed during Hurricane Matthew. However, storms with both heavy rain and large increases in the shoreline water level generate a different cross-island head gradient than ocean storms with no precipitation, which may impact recovery times. Additionally, only rainfall during large offshore waves and surge is considered here. If a large rainstorm precedes a large wave event, the wave-and-surge-driven response might be weaker if the pre-storm water table remains significantly elevated above MSL. Furthermore, surge-driven increases in the water table may inhibit the recovery of the rainfall-driven increases (Bevacqua et al., 2019). Future work should consider how timing of rain and shoreline water level increases impact the groundwater response and how compound rain and shoreline water level increases affect recovery time.

Additionally, groundwater-driven increases in the water table are only one mechanism of flooding in coastal zones. Rainfall can cause flooding independently of groundwater as a result of surface ponding and runoff. Variation in land surface coverage will affect these processes, and areas with high impervious surface coverage are most susceptible to flooding driven by precipitation. Data collected through the iFlood app could be incorporated into studies about the effects of impervious surfaces on flooding patterns. Flooding also can occur via inundation from the ocean if sea levels are elevated enough to overtop the dune. Although no incidences of ocean-side inundation occurred within the study area, roadways were inundated farther south near Ocracoke, and landfall of a major hurricane could cause overtopping and inundation. Even when groundwater is not the primary driver of the flood, the position of the water table will affect flood recovery times, and thus understanding compound effects between these different mechanisms will be important for managing coastal flood hazards.

5.3. *Management of groundwater-flooding on the Outer Banks*

The results suggest that the storm-driven groundwater pulse could flood more than 10% of the ocean-side of the Outer Banks during an event with a 2.25 m increase in shoreline water level (e.g., 1.00 m storm surge and 6.25 m waves) without precipitation (Fig. 11). This estimate is conservative because the initial water-table distribution was designed to represent the aquifer under calm ocean conditions. The extent of flooding across the barrier would be more severe if the water table had not recovered from a prior storm or rainfall. Additionally, groundwater-driven flooding is likely to increase as the water table increases with rising sea levels (Bjerklie et al., 2012). Global sea level is predicted to rise between 0.5 and 1.4 m by 2100, and sea level rise along the Atlantic Coast is predicted to outpace the global estimate (Sweet et al., 2017, Sweet et al., 2020). Consequently, owing to sea level rise and the increasing intensity and duration of North Atlantic storms (Patricola and Wehner, 2018; Knutson et al., 2020), coastal groundwater-driven flooding is expected to present a persistent coastal management challenge.

Structural protections, such as seawalls, jetties, and dikes have been the preferred approach to coastal flood prevention (Dugan et al., 2008; Gittman et al., 2015). Although these protections are effective at mitigating surface water inundation driven by surge, waves, and tides, they do not impede flooding driven by groundwater (Rotzoll and Fletcher, 2013). Additionally, the presence of hardened structures can block the groundwater discharging to the ocean, prolonging the post-storm recovery of the water table (Lee et al., 2019). Flood recovery time is important for assessing the duration of impairment of infrastructure and the vulnerability to future flooding (Chisolm and Matthews, 2012; Lu et al., 2015; Abboud et al., 2018) and should be addressed in future studies.

By understanding the processes contributing to flooding, coastal managers can assess the effectiveness of different flood mitigation strategies. In the town of Nags Head, the iFlood project has reinforced the importance of groundwater levels for flood management. Groundwater flooding is an emerging issue the town has focused on in recent years, and several groundwater-surface-water management projects are being implemented to reduce the frequency and extent of flooding in the town, including a groundwater pumping system used to reduce the water table level in advance of major storms.

5.4. *Use of phone apps for research and increasing community awareness*

iFlood reports extended the scope of the study from a single site, to a 70 km stretch of the Outer Banks between Duck and Rodanthe, NC.

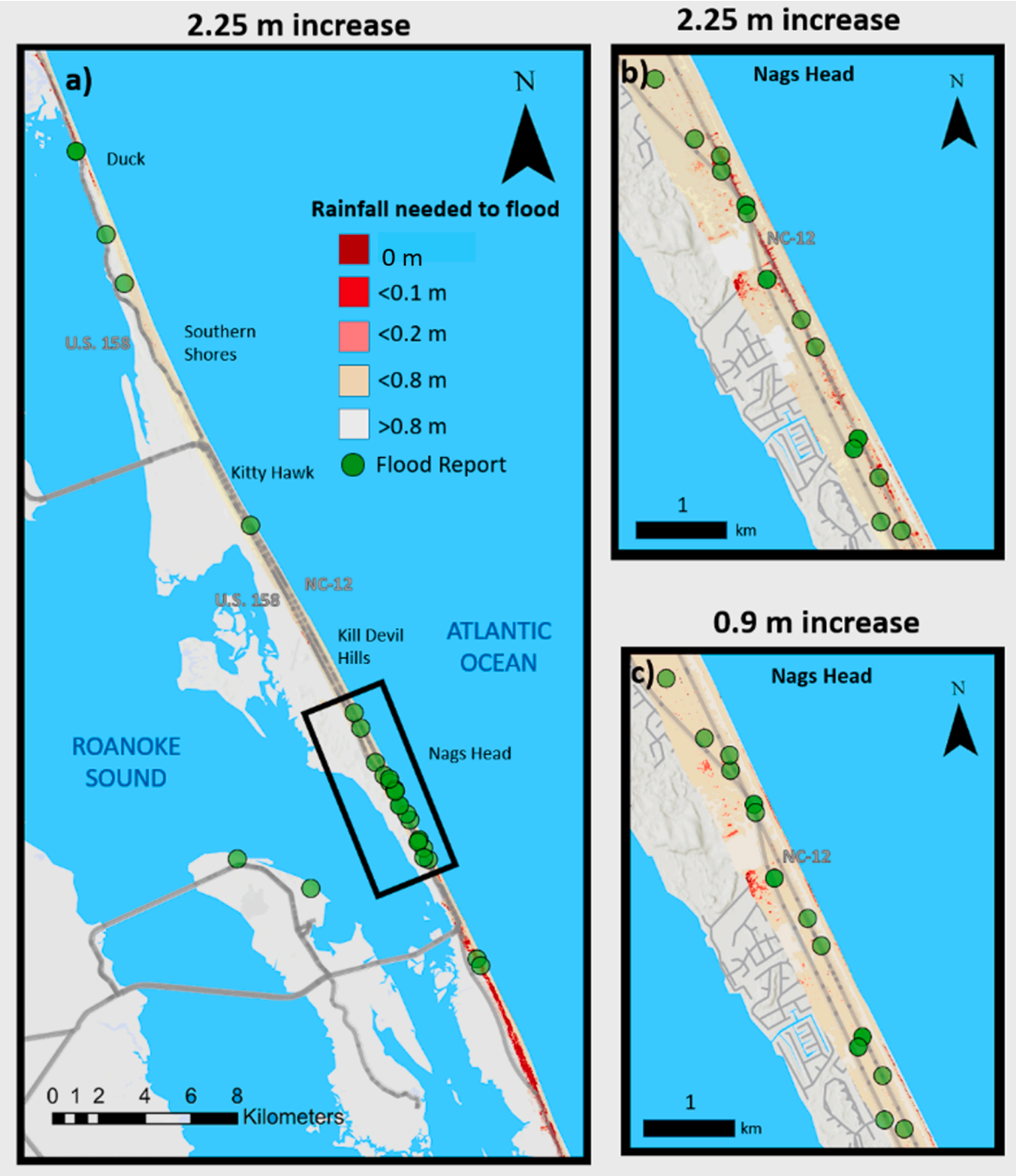

Fig. 11. Maps of flood vulnerability for the extreme storm case (2.25 m shoreline water-level increase) a) from northern Duck to Nags Hag and b) close-up of Nags Head region (black box in panel a), and c) flooding in Nags Head for the moderate storm case (0.9 m shoreline water-level increase).

Although survey responses and photos are used to exclude cases with surface ponding on impermeable surfaces, in some cases the ground surface is difficult to determine. In addition, the phone GPS did not always update automatically, and sometimes it was necessary to use the photo to refine the report location. In cases where photos were not submitted by the user it was more difficult to evaluate the reliability of the flood report. However, the flooding reports and photos provided by the application users enabled evaluation of the model for a large region of the Outer Banks.

The iFlood interface was designed to be simple (i.e., minimal buttons and menus) and accessible (large font, screen reader compatible) to reduce barriers to participation and to help minimize likelihood of accidental submission of inaccurate data. The town managers and USACE FRF personnel were active users of the app and provided a reliable source of flood reports. Nags Head was the region with the highest number of flood reports submitted to iFlood and was one of the partners involved in designing and advertising the iFlood app. Working directly with the town offices enhanced both the quantity and quality of the data received through the app.

Additionally, the citizen-science app increased community awareness of coastal flooding issues and helped town managers identify regions in their communities where there are recurrent flooding issues. The app also enables citizens of the Outer Banks to understand the risks associated with living in a flood-vulnerable environment and to engage with a persistent issue in their communities. Approximately 70 residents attended a public presentation regarding groundwater-induced flooding

and the app, which has been installed over 100 times by users presumed to be local residents. Similar citizen-science approaches could be applied to address other issues related to coastal flooding, and the town of Nags Head plans to use iFlood as a reference to expand the methods the town uses to engage its citizenry and to bring awareness to emerging issues

6. Conclusions

Three years of groundwater level measurements spanning the 550-m-wide barrier island near Duck, NC were used to evaluate an analytical model to predict the response of the water table to surge, wave setup, and precipitation during coastal storms. The groundwater elevation near the ocean increased more than 1 m during storms with large waves and surge, nearly double the magnitude observed in prior studies, resulting in inland-directed head gradients. The bulge of groundwater moved inland causing up to a 0.5 m increase in groundwater levels 310 m inland from the dune. A linear, analytical theory (Li et al., 2004) (without recharge) for the propagation of storm pulses in shallow aquifers reproduces the amplitude attenuation and phase change observed across the island for 26 storm events with minimal rainfall. Nash Sutcliffe Efficiency coefficients are greater than ~0.7 and errors in the modeled maximum water table are less than 0.1 m from the dune to 160 m inland. Infiltration of precipitation results in approximately a threefold increase in the groundwater level relative to the amount of rainfall. The model with recharge reproduces the maximum water table levels within 0.15 m for the single ocean storm with significant rainfall (Hurricane Matthew, Oct 2016).

Citizen-science reports of flooding submitted with a smartphone app, iFlood, were used to evaluate a regional application of the analytical model with recharge along 70-km of the Outer Banks of North Carolina. Between Sept 2019 and Feb 2020, 25 reports on the ocean-side of the island associated with 7 storms showed flooding on natural (pervious) land surfaces between Corolla and Rodanthe, NC. Flooding occurred after storms with large ocean surge and waves, with and without significant rainfall. The analytical model with recharge predicted flooding events that were consistent with the timing and location for 19 of these reports. Additionally, the iFlood app provides a new tool for evaluating groundwater-flooding processes across the North Carolina Outer Banks, and is a framework that can be modified to address a broader range of scientific objectives (e.g., the role of land surface coverage on flooding, sound-driven flooding processes).

The analytical model provides a simple and computationally efficient framework for predicting flooding risk along the ocean-side of the barrier island. For a hypothetical storm with a 2.25 m increase in shoreline water level, the analytical model suggests that more than 10% of the ocean-side of the Outer Banks could be inundated by coastal-groundwater flooding in the absence of rainfall (precipitation would increase the flooding extent).

CRediT authorship contribution statement

Rachel Housego: Funding acquisition, Conceptualization, Methodology, Formal analysis, Visualization, Writing - original draft. **Britt Raubenheimer:** Funding acquisition, Conceptualization, Methodology, Supervision, Writing - review & editing. **Steve Elgar:** Funding acquisition, Conceptualization, Methodology, Supervision, Writing - review & editing. **Sandy Cross:** Conceptualization, Methodology, Investigation. **Christian Legner:** Conceptualization, Methodology, Investigation. **David Ryan:** Conceptualization, Methodology, Investigation.

Declaration of Competing Interest

The authors declare that they have no known competing financial interests or personal relationships that could have appeared to influence the work reported in this paper.

Acknowledgements

We thank the USACE CHL-Field Research Facility for ocean and meteorological observations, Levi Gorrell, Fred Marin, Emmett Krupczak, Heidi Wadman, Jesse McNinch, and Pat Dickhudt for assistance deploying and maintaining the groundwater wells, and Kent Hathaway for assistance with precipitation data. We also thank the users of the iFlood app who contributed flood reports to this project, and we thank two anonymous reviewers for their insightful comments that greatly improved the manuscript. Funding was provided by the U.S. Coastal Research Program, the National Science Foundation, a National Science Foundation Graduate Research Fellowship, the Woods Hole Oceanographic ISP program, and a Vannevar Bush Faculty Fellowship.

Appendix A. Analytical groundwater pulse model

The spatial and temporal evolutions of the storm-driven groundwater pulse are simulated using the analytical solution (Li et al., 2004):

$$h(x,t) = -2AB\int_{-\infty}^{t}(\varepsilon - t_p)exp\left[-B(\varepsilon - t_p)^2\right]erfc\left[\frac{x}{\sqrt{D(t-\varepsilon)}}\right]d\varepsilon \quad (A1)$$

where h is the groundwater level (m), x is the cross-shore position (m, positive inland from the x0 well), t is time (d) after the start of the storm (defined as the local minima in head level at x0 preceding the storm), A is the amplitude of the x0 fluctuation (m), B is a time factor (d^{-2}, $B^{-1/2}$ represents the duration of the elevated water level at x0), t_p is the time of the storm peak at x0 relative to the preceding local minima, and D is aquifer diffusivity (m^2/d). The analytical solution assumes a homogeneous and isotropic aquifer, consistent with the results of the slug tests that were performed across the barrier island. The analytical solution also assumes a shallow aquifer, unidirectional (horizontal) flow, negligible capillary effects, small pulse amplitude relative to aquifer depth, and a vertical beach.

In addition to time series comparisons, the analytical solution is evaluated by comparison with the observed amplitude A_j and time of peak water level $t_{p,j}$ (the local maxima in head after time t_0, which ranged from 1 to 9 d) at inland locations j. The observed 36-hr averaged groundwater fluctuation h_j at each location is fit using least squares to a pulse function

$$h_j(t) = h_{0_j} + A_j exp\left[-B_j\left(t - t_{p_j}\right)\right] \quad (A2)$$

where h_{0_j} is the pre-storm head level and A_j and B_j are the pulse amplitude and time factors, respectively. Only the increasing portion of the groundwater level time series is used in the fit because the temporal asymmetry of the draining relative to the filling of the unconfined aquifer often is not consistent with the Gaussian pulse assumed by the analytical solution (Cartwright and Gibbes, 2011). The resulting squared correlations (R^2) for

the fits are greater than 0.9 for all storms at all locations. Hurricane Matthew is excluded from the pulse propagation analysis because groundwater changes owing to rainfall of 0.2 m obscured the groundwater fluctuation driven by the increase in shoreline water level.

To estimate analytically the pulse amplitude and time lag as a function of inland position, Equation (A1) is non-dimensionalized as:

$$h^*(x^*,t^*) = -2\int_{-\infty}^{t^*} \varepsilon^* exp\left[-(\varepsilon^*)^2\right] erfc\left[\frac{x^*}{\sqrt{t^*-\varepsilon^*}}\right] d\varepsilon^* \quad (A3)$$

in which the non-dimensional amplitude attenuation (α), time lag ($\Delta\phi_*$), time (t^*), and cross-shore location (x^*) at inland locations j computed relative to the x0 well are given by Li et al. (2004):

$$\alpha = \frac{A_j}{A} \quad (A4)$$

$$\Delta\phi^* = \left(t_{p_j} - t_p\right)\sqrt{B} \quad (A5)$$

$$t^* = \left(t - t_p\right)\sqrt{B} \quad (A6)$$

$$x^* = \frac{x}{2\sqrt{D/B^{1/2}}} \quad (A7)$$

The aquifer diffusivity is estimated by determining the value that yields the best fit of the analytical solution (Equation (A1)) to the observed water table fluctuation and to the observed non-dimensional amplitude attenuation and phase lag (Equations (A4) and (A5)) as a function of non-dimensional distance (Equation (A7)) for the 26 storm events without heavy rainfall (both estimates give similar values for D).

The effects of rainfall are accounted for in the pulse model assuming linear superposition to yield the analytical model with recharge:

$$h(x,t) = h_{0,j} - 2AB\int_{-\infty}^{t} (\varepsilon - t_p) exp\left[-B(\varepsilon - t_p)^2\right] erfc\left[\frac{x}{2\sqrt{D(t-\varepsilon)}}\right] d\varepsilon + \frac{R}{n_e} \quad (A8)$$

where the amount of rainfall during the storm R is assumed spatially uniform and n_e is the effective porosity estimated from observations.

References

Abarca, E., Karam, H., Hemond, H., Harvey, C., 2013. Transient groundwater dynamics in a coastal aquifer: The effects of tides, the lunar cycle, and the beach profile. Water Resour. 49, 2473–2488. https://doi.org/10.1002/wrcr.20075.

Abboud, J.M., Ryan, M.C., Osborn, G.D., 2018. Groundwater flooding in a river-connected alluvial aquifer. J. Flood Risk Manag. 11, e12334 https://doi.org/10.1111/jfr3.12334.

Anderson, W.P., Evans, D.G., Snyder, S.W., 2000. The effects of Holocene barrier-island evolution on water-table elevations, Hatteras Island, North Carolina. USA. Hydrogeol. J. 8, 390–404. https://doi.org/10.1007/s100400000081.

Anderson, W.P.J., Lauer, R.M., 2008. The role of overwash in the evolution of mixing zone morphology within barrier islands. Hydrogeol. J. 16, 1483–1495. https://doi.org/10.1007/s10040-008-0340-z.

Befus, K.M., Barnard, P.L., Hoover, D.J., Finzi Hart, J.A., Voss, C.I., 2020. Increasing threat of coastal groundwater hazards from sea-level rise in California. Nat. Clim. Chang. 10, 946–952. https://doi.org/10.1038/s41558-020-0874-1.

Bevacqua, E., Maraun, D., Vousdoukas, M.I., Voukouvalas, E., Vrac, M., Mentaschi, L., Widmann, M., 2019. Higher probability of compound flooding from precipitation and storm surge in Europe under anthropogenic climate change. Sci. Advances Climatol. 5. https://doi.org/10.1126/sciadv.aaw553.

Bjerklie, D.M., Mullaney, J.R., Stone, J.R., Skinner, B.J., Ramlow, M.A., 2012. Preliminary investigation of the effects of sea-level rise on groundwater levels in New Haven. Connecticut. U.S, Geologic Survey.

Boss, S.K., Hoffman, C.W., Cooper, B., 2002. Influence of fluvial processes on the quaternary geologic framework of the continental shelf, North Carolina. USA. Mar. Geol. 183, 45–65. https://doi.org/10.1016/S0025-3227(01)00253-5.

Bouwer, H., Rice, R.C., 1976. A slug test for determining hydraulic conductivity of unconfined aquifers with completely or partially penetrating wells. Water Resour. Res. 12, 423–428. https://doi.org/10.1029/WR012i003p00423.

Broadbridge, P., White, I., 1988. Constant rate rainfall infiltration: A versatile nonlinear model: 1. Analytic solution. Water Resour. Res. 24, 145–154. https://doi.org/10.1029/WR024i001p00145.

Browder, A.G., McNinch, J.E., 2006. Linking framework geology and nearshore morphology: Correlation of paleo-channels with shore-oblique sandbars and gravel outcrops. Mar. Geol. 231, 141–162. https://doi.org/10.1016/j.margeo.2006.06.006.

Brown, D.L., Narasimhan, T.N., Demir, Z., 1995. An Evaluation of the Bouwer and Rice Method of slug test analysis. Water Resour. Res. 31, 1239–1246. https://doi.org/10.1029/94WR03292.

Butler, J.J., McElwee, C.D., Liu, W., 1996. Improving the quality of parameter estimates obtained from slug tests. Ground Water 34, 480–490. https://doi.org/10.1111/j.17456584.1996.tb02029.x.

Caldwell, W., 2001. Hydrologic and salinity characteristics of Currituck Sound and selected tributaries in North Carolina and Virginia, 1998-99. USGS, Raleigh NC10.3133/wri014097.

Cartwright, N., Li, L., Nielsen, P., 2004. Response of the salt–freshwater interface in a coastal aquifer to a wave-induced groundwater pulse: field observations and modelling. Adv. Water Resour. 27, 297–303. https://doi.org/10.1016/j.advwatres.2003.12.005.

Cartwright, N., Gibbes, B., 2011. Oceanic pulse forcing of a beach groundwater system. Engineers Australia.

Chisolm, E.I., Matthews, J.C., 2012. Impact of hurricanes and flooding on buried infrastructure. Leadersh. Manag. Eng. 12, 151–156. https://doi.org/10.1061/(ASCE)LM.1943-5630.0000182.

Cobby, D., Morris, S., Parkes, A., Robinson, V., 2009. Groundwater flood risk management: advances towards meeting the requirements of the EU floods directive. J. Flood Risk Manag. 2, 111–119. https://doi.org/10.1111/j.1753-318X.2009.01025.x.

Colyar, M. A., 2016. The influence of tides, waves, and overtopping on the near-shore water table. UC Irvine. ProQuest ID: Colyar_uci_0030M_14174. Merritt ID: ark:/13030/m5km40sp.

Crosbie, R.S., Binning, P., Kalma, J.D., 2005. A time series approach to inferring groundwater recharge using the water-table fluctuation method. Water Resour. Res. 41, 1–9. https://doi.org/10.1029/2004WR003077.

Dugan, J.E., Hubbard, D.M., Rodil, I.F., Revell, D.L., Schroeter, S., 2008. Ecological effects of coastal armoring on sandy beaches. Mar. Ecol. 29, 160–170. https://doi.org/10.1111/j.1439-0485.2008.00231.x.

Elko, N.A., Sallenger, A.H., Guy, K., Stockdon, H.F., Morgan, K.L.M., 2002. Barrier island elevations relevant to potential storm impacts: 1. Techniques. US Geological Survey Open File Report 02–287.

Elko, N., Feddersen, F., Foster, D., Hapke, C., McNinch, J., Mulligan, R., Tuba Özkan-Haller, H., Plant, N., Raubenheimer, B., 2015. The future of nearshore processes research. Shore & Beach 83 (1).

Elko, N., Dietrich, C., Cialone, M.A., Stockdon, H., Bilskie, M.W., Boyd, B., Charbonneau, B., Cox, D., Dresback, K., Elgar, S., Lewis, A., Limber, P., Long, J., Massey, C., Mayo, T., McIntosh, K., Nadal-Caraballo, N.C., Raubenheimer, B., Tomiczek, T., Wargula, A.E., 2019. Advancing the understanding of storm processes and impacts. Shore & Beach 87 (1).

FEMA, Hydrologic analysis of Hurricane Matthew's impact on dam safety in North Carolina and South Carolina, 2018.

Fofonoff, N., Millard Jr., R.C., 1983. Algorithms for the computation of fundamental properties of seawater. UNESCO Tech. Pap. Mar, Sci.

Gittman, R.K., Fodrie, F.J., Popowich, A.M., Keller, D.A., Bruno, J.F., Currin, C.A., Peterson, C.H., Piehler, M.F., 2015. Engineering away our natural defenses: an analysis of shoreline hardening in the US. Front. Ecol. Environ. 13, 301–307. https://doi.org/10.1890/150065.

Glover, R.E., 1959. The pattern of fresh-water flow in a coastal aquifer. J. Geophys. Res. 64, 457–459. https://doi.org/10.1029/jz064i004p00457.

Guza, R.T., Thornton, E.B., 1981. Wave set-up on a natural beach. J. Geophys. Res. 86, 4133. https://doi.org/10.1029/JC086iC05p04133.

Horn, D., Webel, B., 2019. Introduction to the National Flood Insurance Program (NFIP). Congressional Research Service. R44593. https://fas.org/sgp/crs/homesec/R44593.pdf.

Huang, F.K., Chuang, M.H., Wang, G.S., Yeh, H.D., 2015. Tide-induced groundwater level fluctuation in a U-shaped coastal aquifer. J. Hydrol. 530, 291–305. https://doi.org/10.1016/j.jhydrol.2015.09.032.

Hvorslev, M.J., 1951. Time lag and soil permeability in ground-water observations, Waterways Experiment Station, Corps of Engineers. U. S. Army, Bull. 36, 49.

Knutson, T., Camargo, S.J., Chan, J.C.L., Emanuel, K., Ho, C.H., Kossin, J., Mohapatra, M., Satoh, M., Sugi, M., Walsh, K., Wu, L., 2020. Tropical cyclones and climate change assessment part II: Projected response to anthropogenic warming. Bull. Am. Meteorol. Soc. 101, E303–E322. https://doi.org/10.1175/BAMS-D-18-0194.1.

Lautier, J.C., 2009. Hydrogeologic framework and ground water conditions in the North Carolina East Central Coastal Plain. North Carolina Department of Environment and Natural Resources, Division of Water Resources.

Lazarus, E.D., Murray, A.B., 2011. An integrated hypothesis for regional patterns of shoreline change along the Northern North Carolina Outer Banks. USA. Mar. Geol. 281, 85–90. https://doi.org/10.1016/j.margeo.2011.02.002.

Lee, W.D., Yoo, Y.J., Jeong, Y.M., Hur, D.S., 2019. Experimental and numerical analysis on hydraulic characteristics of coastal aquifers with seawall. Water 11, 2343. https://doi.org/10.3390/w11112343.

Li, L., Barry, D.A., Cunningham, C., Stagnitti, F., Parlange, J.Y., 2000. A two-dimensional analytical solution of groundwater responses to tidal loading in an estuary and ocean. Adv. Water Resour. 23, 825–833. https://doi.org/10.1016/S0309-1708(00)00016-6.

Li, L., Cartwright, N., Nielsen, P., Lockington, D., 2004. Response of coastal groundwater table to offshore storms. China Ocean Engi. 18 (3), 423–431.

Longuet-Higgins, M.S., Stewart, R.W., 1964. Radiation stresses in water waves; a physical discussion, with applications. Deep. Res. 11, 529–562.

Lu, Q.C., Peng, Z.R., Zhang, J., 2015. Identification and prioritization of critical transportation infrastructure: Case study of coastal flooding. J. Transp. Eng. 141 https://doi.org/10.1061/(ASCE)TE.1943-5436.0000743.

MacDonald, D.M.J., Bloomfield, J.P., Hughes, A.G., MacDonald, A.M., Adams, B., McKenzie, A.A., 2008. Improving the understanding of the risk from groundwater flooding in the UK. British Geol. Surv. UK. In: Proceedings of Flood Risk European Conference on Flood Risk Management, Oxford, September 2008. CRC Press, the Netherlands.

Mallinson, D., Smith, C.W., Culver, S.J., Riggs, S.R., Ames, D., 2010. Geological characteristics and spatial distribution of paleo-inlet channels beneath the outer banks barrier islands, North Carolina, USA. Estuar. Coast. Shelf Sci. 88, 175–189. https://doi.org/10.1016/j.ecss.2010.03.024.

Manahan, S., Martin, W.K., Guo, W., 1998. Dare County-wide hydrogeological study and groundwater resource evaluation. Dare Cty. Water Prod. Dep, Kill Devil Hills, NC.

Meinzer, O., 1923. The occurrence of ground water in the United States with a discussion of principles. U.S. Geol. Survey Water-Supply Paper 489, 321.

Meisburger, E.P., Williams, S.J., Judge, C., 1989. Physiographic and geological setting of the Coastal Engineering Research Center's Field Research Facility. Vicksburg, MS.

Moftakhari, H.R., AghaKouchak, A., Sanders, B.F., Feldman, D.L., Sweet, W., Matthew, R. A., Luke, A., 2015. Increased nuisance flooding along the coasts of the United States due to sea level rise: Past and future. Geophys. Res. Lett. 42, 9846–9852. https://doi.org/10.1002/2015GL066072.

Morris, S.E., Cobb, D., Parkes, A., 2007. Towards groundwater flood risk mapping. Q. J. Eng. Geol. Hydrogeol. 40, 203–211.

Mulligan, R.P., Walsh, J.P., Wadman, H.M., 2014. Storm surge and surface waves in a shallow lagoonal estuary during the crossing of a hurricane. J. Waterw. Port, Coastal. Ocean Eng. 141, A5014001. https://doi.org/10.1061/(ASCE)WW.1943-5460.0000260.

Nash, J.E., Sutcliffe, J.V., 1970. River flow forecasting through conceptual models part I—A discussion of principles. Journal of hydrology 10 (3), 282–290.

Nielsen, P., 1988. Wave setup: A field study. J. Geophys. Res. 93, 15643. https://doi.org/10.1029/JC093iC12p15643.

Nielsen, P., 1990. Tidal dynamics of the water table in beaches. Water Resour. Res. 26, 2127–2134. https://doi.org/10.1029/WR026i009p02127.

Patricola, C.M., Wehner, M.F., 2018. Anthropogenic influences on major tropical cyclone events. Nature 563, 339–346. https://doi.org/10.1038/s41586-018-0673-2.

Post, V., Kooi, H., Simmons, C., 2007. Using hydraulic head measurements in variable-density ground water flow analyses. Groundwater 45 (6), 664–671.

Raubenheimer, B., Guza, R.T., Elgar, S., 1999. Tidal water table fluctuations in a sandy ocean beach. Water Resour. Res. 35 (8), 2313–2320.

Raubenheimer, B., Guza, R.T., Elgar, S., 2001. Field observations of wave-driven setdown and setup. J. Geophys. Res. Ocean. 106, 4629–4638. https://doi.org/10.1029/2000JC000572.

Riggs, S.R., Cleary, W.J., Snyder, S.W., 1995. Influence of inherited geologic framework on barrier shoreface morphology and dynamics. Mar. Geol. 126, 213–234. https://doi.org/10.1016/0025-3227(95)00079-E.

Rotzoll, K., El-Kadi, A.I., 2008. Estimating hydraulic properties of coastal aquifers using wave setup. J. Hydrol. 353, 201–213. https://doi.org/10.1016/j.jhydrol.2008.02.005.

Rotzoll, K., El-Kadi, A.I., Gingerich, S.B., 2008. Analysis of an unconfined aquifer subject to asynchronous dual-tide propagation. Groundwater 46 (2), 239–250.

Rotzoll, K., Fletcher, C.H., 2013. Assessment of groundwater inundation as a consequence of sea-level rise. Nat. Clim. Chang. 3, 477–481. https://doi.org/10.1038/nclimate1725.

Smail, R.A., Pruitt, A.H., Mitchell, P.D., Colquhoun, J.B., 2019. Cumulative deviation from moving mean precipitation as a proxy for groundwater level variation in Wisconsin. J. Hydrol. X 5, 100045. https://doi.org/10.1016/j.hydroa.2019.100045.

Stutz, M., Pilkey, O., 2011. Open-ocean barrier islands: global influence of climatic, oceanographic, and depositional settings. J. Coast. Res. 27 (2), 207–222.

Sweet, W., Kopp, R., Weaver, C.P., Obeysekera, J.T.B., Horton, R.M., Thieler, E.R., Zervas, C.E., 2017. NOAA Technical Report NOS CO-OPS 083 Global and regional sea level rise scenarios for the United Stat.

Sweet, W., Dusek, G., Carbin, G., Marra, J., Marcy, D., Simon, S., 2020. NOAA Technical Report NOS CO-OPS 092. National Oceanic and Atmospheric Administration 2019 State of U.S. High Tide Flooding with a 2020 Outlook.

Trefry, M.G., Bekele, E., 2004. Structural characterization of an island aquifer via tidal methods. Water Resour. Res. 40 (1) https://doi.org/10.1029/2003WR002003.

Trglavcnik, V., Morrow, D., Weber, K.P., Li, L., Robinson, C.E., 2018. Analysis of tide and offshore storm-induced water table fluctuations for structural characterization of a coastal island aquifer. Water Resour. Res. 54 (4) https://doi.org/10.1002/2017WR020975.

Vitousek, S., Barnard, P.L., Fletcher, C.H., Frazer, N., Erikson, L., Storlazzi, C.D., 2017. Doubling of coastal flooding frequency within decades due to sea-level rise. Sci. Rep. 7, 1–9. https://doi.org/10.1038/s41598-017-01362-7.

Vousdoukas, M.I., Ranasinghe, R., Mentaschi, L., Plomaritis, T.A., Athanasiou, P., Luijendijk, A., Feyen, L., 2020. Sandy coastlines under threat of erosion. Nat. clim. change 10 (3), 260–263.

Wahl, T., Jain, S., Bender, J., Meyers, S.D., Luther, M.E., 2015. Increasing risk of compound flooding from storm surge and rainfall for major US cities. Nat. Clim. Chang. 5, 1093–1097. https://doi.org/10.1038/nclimate2736.

Winner, M.D.J., Coble, R., 1996. Hydrogeologic framework of the North Carolina Coastal Plain No, 1404-I).

Woodruff, J., Irish, J., Camargo, S.J., 2013. Coastal flooding by tropical cyclones and sea-level rise. Nature 504, 44–52. https://doi.org/10.1038/nature12855.

Zhang, K., Leatherman, S., 2011. Barrier island population along the U.S. Atlantic and Gulf coasts. J. Coast. Res. 272, 356–363. https://doi.org/10.2112/JCOASTRES-D-10-00126.1.

Zhang, M., Singh, H.V., Migliaccio, K.W., Kisekka, I., 2017. Evaluating water table response to rainfall events in a shallow aquifer and canal system. Hydrol. Process. 31, 3907–3919. https://doi.org/10.1002/hyp.11306.